BIOCHEMISTRY
including biophysical chemistry & molecular biology

Article

pubs.acs.org/biochemistry

Interplay of the H-Bond Donor−Acceptor Role of the Distal Residues in Hydroxyl Ligand Stabilization of *Thermobifida fusca* Truncated Hemoglobin

Francesco P. Nicoletti,[†,○,▽] Juan P. Bustamante,[‡,§,○] Enrica Droghetti,[†] Barry D. Howes,[†] Maria Fittipaldi,[∥] Alessandra Bonamore,[⊥] Paola Baiocco,[#] Alessandro Feis,[†] Alberto Boffi,[⊥] Darío A. Estrin,[‡] and Giulietta Smulevich*[,†]

[†]Dipartimento di Chimica "Ugo Schiff", Università di Firenze, Via della Lastruccia 3-13, I-50019 Sesto Fiorentino (FI), Italy

[‡]Departamento de Química Inorgánica, Analítica y Química Física/INQUIMAE-CONICET, [§]Departamento de Química Biológica, Facultad de Ciencias Exactas y Naturales, Universidad de Buenos Aires, C1428EHA Buenos Aires, Argentina

[∥]INSTM and Dipartimento di Fisica e Astronomia, Università degli Studi di Firenze, via Sansone 1, I-50019 Sesto Fiorentino, Italy

[⊥]Institute Pasteur, Fondazione Cenci Bolognetti, Department of Biochemical Sciences and CNR, Institute of Molecular Biology and Pathology, University of Rome "La Sapienza", Piazzale Aldo Moro 5, I-00185 Rome, Italy

[#]Center of Life Nano Sciences, Italian Institute of Technology, Viale Regina Elena 291, I-00161 Rome, Italy

Supporting Information

ABSTRACT: The unique architecture of the active site of *Thermobifida fusca* truncated hemoglobin (Tf-trHb) and other globins belonging to the same family has stimulated extensive studies aimed at understanding the interplay between iron-bound ligands and distal amino acids. The behavior of the heme-bound hydroxyl, in particular, has generated much interest in view of the relationships between the spin-state equilibrium of the ferric iron atom and hydrogen-bonding capabilities (as either acceptor or donor) of the OH^- group itself. The present investigation offers a detailed molecular dynamics and spectroscopic picture of the hydroxyl complexes of the WT protein and a combinatorial set of mutants, in which the distal polar residues, TrpG8, TyrCD1, and TyrB10, have been singly, doubly, or triply replaced by a Phe residue. Each mutant is characterized by a complex interplay of interactions in which the hydroxyl ligand may act both as a H-bond donor or acceptor. The resonance Raman stretching frequencies of the Fe−OH moiety, together with electron paramagnetic resonance spectra and MD simulations on each mutant, have enabled the identification of specific contributions to the unique ligand-inclusive H-bond network typical of this globin family.

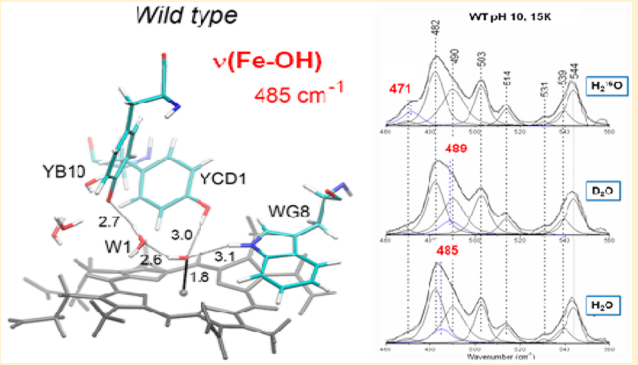

Heme proteins are a ubiquitous family of metallo-proteins containing heme as a prosthetic group. In spite of the fact that all heme proteins share the same active site, they display an amazing variety of behaviors that makes them an excellent benchmark for the investigation of the relationship between protein structure and function. In this context, the currently available heme spectroscopic data provide the scientific foundation upon which functional and biological paradigms of heme proteins can be validated or challenged. Understanding heme protein spectroscopy thus allows one to translate physicochemical properties of the active site into the observed functional behavior. X-ray crystallography has provided fundamental snapshots of active site structural frameworks and highlighted the network of interactions that contributes to modulate the functional properties of the macromolecule around the metal binding site. On the basis of X-ray diffraction data and static or dynamic spectroscopic observations, it is now clear that iron-bound ligands in the heme binding pocket experience a network of electrostatic fields and hydrogen-bonding interactions exerted by nearby amino acid side chains.[1] In fact, specific short-range amino acid side chain interactions with ligands appear to contribute to the diversity of heme protein functional behavior at a level of structural detail that is not always achievable even with high-resolution crystallographic data, which is typically restricted to one static conformation. Within this framework, cross correlations among structural data, spectroscopic marker bands, and appropriate molecular dynamics (MD) investigations are essential to complete the

Received: September 9, 2014
Revised: November 25, 2014
Published: December 1, 2014

dx.doi.org/10.1021/bi501132a | *Biochemistry* 2014, 53, 8021−8030

picture and provide a reliable structure−function correspondence.[1] Recently, a versatile template has been devised for establishing the structure of the heme iron coordination unit in the truncated hemoglobin family of heme proteins. Such a template is based on the truncated hemoglobin from the actinomyces *Thermobifida fusca* (Tf-trHb), the first identified thermostable truncated hemoglobin.[2] In particular, Tf-trHb exemplifies the structural properties of group II trHbs, as the active site is characterized by a highly polar distal environment in which TrpG8, TyrCD1, and TyrB10 provide three potential H-bond donors in the distal cavity to stabilize the incoming ligands. The role of the residues in key topological positions, namely, G8, CD1, and B10, has been recently addressed in studies carried out on the CO,[3] F^-,[4,5] and HS^-[6] adducts formed with the WT protein and a combinatorial set of mutants, in which the distal polar residues, TrpG8, TyrCD1, and TyrB10, have been singly, doubly, or triply replaced by a Phe residue. These studies revealed that all of the ligands are stabilized by TrpG8 via a strong H-bond and that TyrCD1 is able to interact with CO and fluoride, whereas TyrB10 is not directly involved in the ligand stabilization and plays only a minor role.

More recently, however, we carried out a spectroscopic investigation on the Tf-trHb ferric protein and its triple mutant YB10F-YCD1F-WG8F at neutral and alkaline pH.[7] We found that the hydroxyl ligand does not bind to the triple mutant. In the case of the WT protein, binding gives rise to a six-coordinate low-spin (6cLS) species with a ν(Fe−OH) stretching mode at 485 cm^{-1}, about 65 cm^{-1} lower than the corresponding bands observed for metMb and metHb[8−10] or any other truncated hemoglobin.[11] This anomalous very low frequency strongly supports the presence of several H-bonds formed by the bound hydroxyl with distal residues and water molecules. On the basis of MD simulations, we suggested that the OH^-anion moiety is engaged in three H-bonds at alkaline pH, with TrpG8, TyrCD1, and a water molecule that is in turn H-bonded to TyrB10. Therefore, the OH^- ligand appears to be the only example of the involvement of TyrB10, albeit indirectly, in the stabilization of the exogenous ligand.

The aim of the present work is to determine the contributions of each distal side chain to the overall H-bond network and also to demonstrate the involvement of TyrB10 in the hydroxo stabilization. We have, therefore, studied the mutated proteins, where the polar residues have been systematically singly and doubly mutated to Phe, by UV−vis and RR spectra, at acid and alkaline pH, at room and low temperature, and in combination with EPR spectra and molecular dynamics simulations.

The data will be discussed in terms of the different capability of TyrB10 and TyrCD1 to act as a hydrogen-bond donor or acceptor.

MATERIALS AND METHODS

Sample Preparation. Wild-type (WT) Tf-trHb was expressed as a recombinant protein in *Escherichia coli* cells and purified as described previously.[2,3] The acidic surface variant (ASV) of Tf-trHb differs from the WT protein by mutation of both Phe107 and Arg91 to glutamic acid. These mutations increase protein solubility during recombinant expression, without affecting thermostability or ligand binding properties.[3−5] Therefore, ASV was taken as an engineered scaffold of the WT protein for subsequent generation of site-directed mutants of the distal heme pocket. ASV and WT proteins give rise to identical results. Therefore, in the present work, only the spectra of ASV are shown.

Phosphate salts and glycine were obtained from Merck AG (Darmstadt, Germany). 2-[*N*-Morpholino]ethanesulfonic acid (MES) was purchased from Sigma-Aldrich (Steinheim, Germany). All chemicals were of analytical or reagent grade and were used without further purification. Buffered solutions (0.1 M) were used for experiments at pH 9.8 (glycine), 7.0 (phosphate), and 6.1 (MES). It is noted that, due to their instability at pH 9.8, the WG8F-YB10F and WG8F-YCD1F double mutants were studied at pH 9.1.

The hydroxyl complex in isotopically enriched water was prepared by adding 5 μL of protein, in 0.05 M natural abundance buffer, pH 7, to 60 μL of 0.1 M glycine buffer prepared with D_2O or $H_2{}^{18}O$ to obtain a final pD 10.0 and pH 9.8, respectively. Isotopically enriched water ($H_2{}^{18}O$) (95%) and D_2O (99.8%) were purchased from Cambridge Isotope Laboratories (USA) and Merck AG (Darmstadt, Germany), respectively. All chemicals were of analytical or reagent grade and were used without further purification.

Protein concentrations in the range 10−70 μM were used for the electronic absorption and RR samples. Sample concentrations for low-temperature RR were between 30 and 100 μM. Sample concentrations for electron paramagnetic resonance (EPR) experiments were in the range 130−600 μM. Sample concentrations for UV−vis titrations were about 10 μM. Protein solutions for the titrations were prepared in 0.1 M phosphate buffer, and the pH was adjusted by the addition of a few microliters of 1 M NaOH (for the alkaline pH values) or 1 M citric acid (for the acidic pH values) stock solutions. The protein concentration was determined on the CO derivative in the presence of 10−20 mM sodium dithionite using an extinction coefficient of 174 000 M^{-1} cm^{-1} at 420 nm for Tf-trHb.

Spectroscopic Characterization. Electronic absorption spectra were measured with a double-beam spectrophotometer (Varian Cary 5). RR spectra were measured with excitation at 413.1 nm (Kr+ laser, Coherent, Innova 300C). Experimental conditions are as reported previously.[7]

Absorption spectra were measured both prior to and after RR measurements at room temperature to ensure that no degradation had taken place under the experimental conditions used. All RR measurements were repeated several times under the same conditions to ensure reproducibility. A number of spectra were accumulated and summed in order to improve the signal-to-noise ratio only if no spectral differences were noted. All spectra were baseline-corrected. A curve-fitting program (Lab Calc; Galactic) was used to simulate the spectra using a Lorentzian line shape in order to determine peak bandwidth and positions. The frequencies of the bands were optimized with an accuracy of 1 cm^{-1}, and the bandwidths, with an accuracy of 0.5 cm^{-1}. Bandwidths (full width at half-maximum) varied as follows: 12−14 cm^{-1} in the high-frequency region and 9−12 cm^{-1} for the low-frequency region.

The spectrophotometric titration measurements were performed using a 1 cm path-length cuvette. Spectra were baseline-subtracted, and each spectrum of the titration was corrected by the dilution factor.

EPR spectra were recorded on a Bruker Elexys E500 instrument equipped with a microwave frequency counter. An Oxford Instruments ESR 900 cryostat was used to obtain low temperatures. The spectra were recorded under nonsaturating conditions at 5 K, 1 mW microwave power, and 1 mT

dx.doi.org/10.1021/bi501132a | *Biochemistry* 2014, 53, 8021−8030

modulation amplitude. The *g* values were determined by careful visual inspection of the spectra.

Molecular Dynamics Simulations. The three single (WG8F, YCD1F, and YB10F) and three double (YCD1F-WG8F, YB10F-YCD1F, and YB10F-WG8F) distal site mutant proteins were built and simulated according to a previously reported protocol[7] used for WT and triple mutant proteins. The time of the simulations was 50 ns in each case. All structures were found to be stable during the time scale of the simulations, as is evident from the root-mean-square displacements (RMSD), depicted in Figures S1 and S2, Supporting Information.

A possible scenario is that one or two of the tyrosine residues may be deprotonated. In order to assess this eventuality and, hence, to enable a structural simulation of the protein consistent with the spectroscopic data presented herein, both possibilities were considered through 50 ns simulations of the WT protein. The preparation of the deprotonated tyrosine to use in the simulations considered a normal tyrosine (protonated) from which the H atom was removed to evaluate the partial charges. The charges and parameters for the deprotonated tyrosine were determined by the standard procedure: partial charges were computed using the restricted electrostatic potential (RESP) recipe and DFT electronic structure calculations with the PBE functional and 6-31G** basis sets. Equilibrium distances and angles, as well as force constants, were computed using the same methods and basis set used for computed charges.

RESULTS AND DISCUSSION

A detailed description of the pH-dependent changes has been obtained by the combined analysis of the UV−vis spectra, resonance Raman spectra, and MD simulations. Figure 1 compares the UV−vis and RR spectra of the ASV protein and its single and double mutants at pH 7.0, close to the pK_a value of the acid−alkaline transition (Table 1). At neutral pH values, the UV−vis spectroscopic features of the ASV protein are characteristic of a Fe−OH^- heme (maxima at 541 and 577 nm) together with a 6cHS aquo form (CT1 bands around 498 and 634 nm). Accordingly, the RR spectra are a mixture of six-coordinate high-spin (6cHS) (ν_3 at 1480 cm^{-1} and ν_2 at 1563 cm^{-1}) and 6cLS (ν_3 at 1503 cm^{-1}, ν_2 at 1579 cm^{-1}, ν_{10} at 1638 cm^{-1}) states. A small amount of 5cHS form (ν_3 at 1489 cm^{-1} and ν_2 at 1570 cm^{-1}) is also observed. Classical molecular dynamics simulations performed on the ASV ferric form reveal that the coordinated water is stabilized by strong H-bonds with the indole N proton of the WG8 (H_2O−N_{WG8} = 1.9 Å) and the hydroxylic hydrogen of the YCD1 (O_{H_2O}−O_{YCD1} = 1.5 Å), confirming the spectroscopic findings that suggest a Fe−OH^- character of the ligand even at pH 6.1.[7]

The pK_a of the acid−alkaline transition is an optimum probe of the overall charge distribution in the distal pocket microenvironment of heme proteins characterized by an aquo-met state at neutral pH.[8,12,13] In the case of Tf-trHb and its distal pocket mutants, the pK_a of the acid−alkaline transition has been determined by absorption spectrophotometry. We have monitored both Δ_{634}, the decrease of the absorbance at 634 nm (6cHS aquo), and Δ_{577}, the increase of the absorbance at 577 nm (hydroxo form), as the pH is increased from 6 to 10. The experimental data of Δ_{634} and Δ_{577} were plotted as a function of pH and fitted to the Henderson−Hasselbalch equation. The pK_a values thus determined are shown in Table 1, and the plots are reported in Figure S3, Supporting Information.

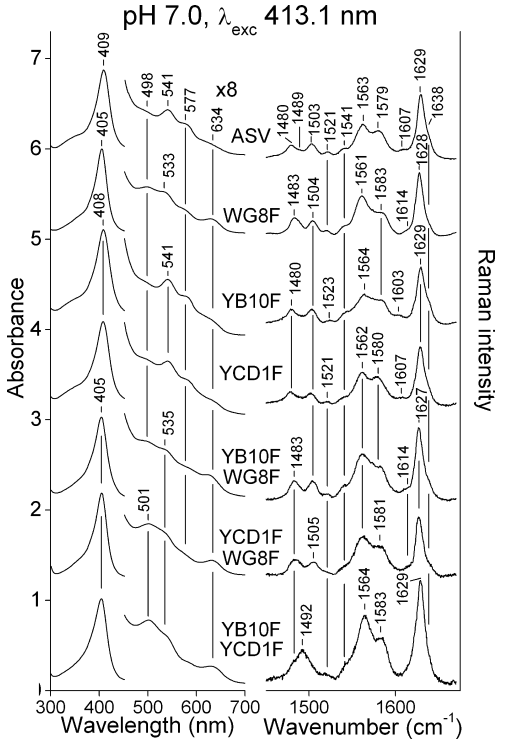

Figure 1. UV−vis (left) and the high-frequency region RR spectra (right) of ASV Tf-trHb and its single and double mutants at pH 7.0. Left: the region between 460 and 700 nm has been expanded 8-fold. Right: 413.1 nm laser excitation; 1 cm^{-1} spectral resolution. RR experimental conditions: ASV: 10 mW laser power at the sample; average of 3 spectra with 240 s integration time. WG8F: 10 mW laser power at the sample; average of 3 spectra with 240 s integration time. YB10F: 14 mW laser power at the sample; average of 7 spectra with 180 s integration time. YCD1F: 6 mW laser power at the sample; average of 4 spectra with 420 s integration time. YB10F-WG8F: 6 mW laser power at the sample; average of 8 spectra with 300 s integration time. YCD1F-WG8F: 6 mW laser power at the sample; average of 4 spectra with 360 s integration time. YB10F-YCD1F: 3 mW laser power at the sample; average of 2 spectra with 240 s integration time. Spectra have been shifted along the ordinate axis to allow better visualization.

Table 1. Calculated pK_a Values for the Alkaline Transition of WT Tf-trHb and Its Distal Mutants[a]

	pK_a A_{634}	pK_a A_{577}
WT/ASV	7.3	7.4
WG8F	8.0	8.7
YCD1F	7.1	7.0
YB10F	6.7	7.1
YB10F-YCD1F	8.2	7.8
WG8F-YB10F	8.6	8.7
WG8F-YCD1F	8.1	8.5

[a]The maximum error in the pK_a values is ±0.2.

The observed pK_a value for the acid−alkaline transition of the ASV protein (pH 7.4) is much lower than that observed in classical vertebrate globins (near 9.0).[14] As expected, the pK_a of the transition is sensitive to the presence of the WG8 residue. When Trp is mutated to Phe (WG8F, WG8F-YB10F, and WG8F-YCD1F mutants), the pK_a increases by about 1 unit. A similar effect, although less marked, is also observed in the

dx.doi.org/10.1021/bi501132a | *Biochemistry* 2014, 53, 8021−8030

absence of both tyrosines in the double YB10F-YCD1F mutant, whereas a single Tyr mutation (YCD1F or YB10F mutants) shows only a minor effect.

In agreement with the pK_a values (Table 1), the spectral characteristics of the hydroxo species are maintained only in the single YCD1F and YB10F mutants at pH 7.0 (Figure 1). In contrast, the population of hydroxo-ligated proteins appears to be drastically decreased in the mutants lacking the WG8 residue (WG8F, YB10F-WG8F, YCD1-WG8F). In the absence of WG8, a blue shift of the Soret band to 405 nm, the appearance of the intense band at 498 nm (501 nm in the YCD1-WG8F), and the relative increase of the RR bands due to the 6cHS aquo (ν_3 at 1483 cm^{-1}) are observed. These changes strongly indicate that H-bond donation by the WG8 indole N proton plays a critical role in the stabilization of the anionic hydroxo ligand. However, the ancillary H-bonds of the tyrosines are highlighted by the formation of a 5cHS form (ν_3 at 1492 cm^{-1}) in the YB10F-YCD1F double mutant.

At more acidic pH values (around 6.0), the population of the 6cHS form increases at the expense of the 6cLS state for ASV[7] and the YB10F and YCD1F mutants, whereas the UV−vis spectra of all other proteins remain unchanged (Figure S4, Supporting Information). These observations are confirmed by the EPR spectra shown in Figure 2. At pH 6.0, the high-spin

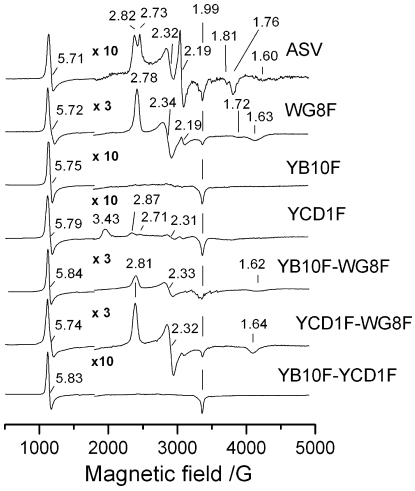

Figure 2. X-band EPR spectra of Tf-trHb and mutants at pH 6.0 in 0.1 M MES. The spectra were recorded at 5 K, 1 mW microwave power, and 10 G modulation amplitude. Spectra have been shifted along the ordinate axis to allow better visualization. *g* values are indicated, as well as the multiplication factor of the high-field part of the spectrum compared with the low-field part.

bands of the mutants show a variable degree of rhombicity, which is likely due to the mixture of a 6cHS state and a variable amount of a minor 5cHS species. Figure S5A (Supporting Information) compares the case for ASV and the YB10F-WG8F double mutant. The latter displays a more axial signal than ASV, indicating an enhanced contribution of the 6cHS species. The LS species represents a negligible contribution to the spectrum, in agreement with the UV−vis spectra at pH 6.0 (Figure S4, Supporting Information).

Similar to Hb and Mb,[8] the absorption spectrum of ASV at pH 9.8 (Figure 3) is characterized by a Soret band at 413 nm, Q bands at 545 and 577 nm, and a CT1 band at around 609 nm, indicating that the hydroxide derivative is a mixture of 6cHS and 6cLS hemes. Accordingly, at room temperature, the

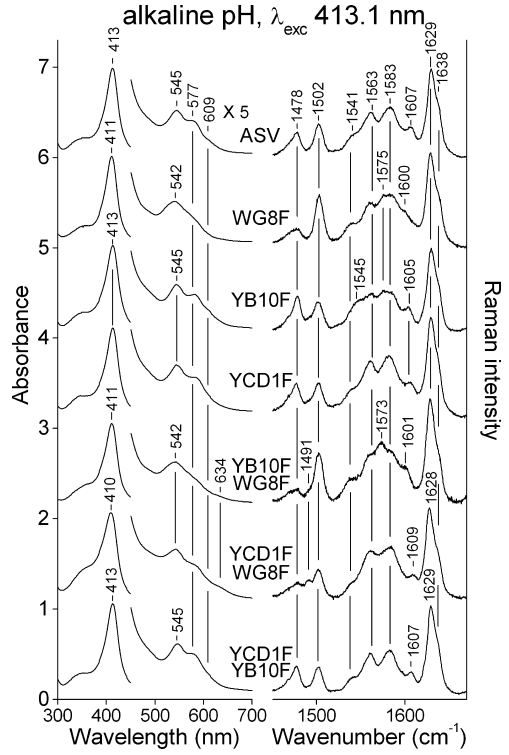

Figure 3. UV−vis (left) and the high-frequency region RR spectra (right) of ASV Tf-trHb and its single and double mutants at pH 9.8, except for WG8F-YB10F and WG8F-YCD1F (pH 9.1). Left: the region between 460 and 700 nm has been expanded 5-fold. Right: 413.1 nm laser excitation; 1 cm^{-1} spectral resolution. Experimental conditions: ASV: 10 mW laser power at the sample; average of 2 spectra with 240 s integration time. WG8F: 14 mW laser power at the sample; average of 2 spectra with 400 s integration time. YB10F: 15 mW laser power at the sample; average of 5 spectra with 200 s integration time. YCD1F: 17 mW laser power at the sample; average of 9 spectra with 200 s integration time. YB10F-WG8F: 4 mW laser power at the sample; average of 5 spectra with 360 s integration time. YCD1F-WG8F: 3 mW laser power at the sample; average of 2 spectra with 600 s integration time. YB10F-YCD1F: 15 mW laser power at the sample; average of 2 spectra with 240 s integration time. Spectra have been shifted along the ordinate axis to allow better visualization.

high-frequency region of the RR spectra displays two sets of core size marker bands corresponding to the 6cHS (ν_3 at 1478 cm^{-1}, ν_2 at 1563 cm^{-1}, ν_{10} at 1607 cm^{-1}) and 6cLS (ν_3 at 1502 cm^{-1}, ν_2 at 1583 cm^{-1}, ν_{10} at 1638 cm^{-1}) hydroxo forms. The two forms, which exist in a thermal spin-state equilibrium at room temperature, convert to an almost pure 6cLS heme at 15 K (ν_3 at 1505 cm^{-1}, ν_2 at 1588 cm^{-1}, ν_{10} at 1642 cm^{-1}) (Figure S6, Supporting Information).[7]

Figure 4 shows the low-frequency region RR spectra at alkaline pH at 298 (left) and 15 K (right). Unlike the high-frequency region, major changes are observed in the ν(Fe−OH) stretching frequency (assigned on the basis of the curve-fitted spectra and the isotopic substitution in D_2O and $H_2{}^{18}O$ buffers; see Figure S7, Supporting Information) upon mutation.

It must be noted that the calculated values reported in Table 2 for the isotopic shift in $H_2{}^{18}O$ and D_2O correspond to the ideal value, assuming that the two oscillating units are the Fe and the OH in an isolated Fe−OH harmonic oscillator. When the OH group has strong hydrogen-bonding interactions with its neighboring groups, the expected isotope shift may be different because of the deviation from a perfect two-body

dx.doi.org/10.1021/bi501132a | *Biochemistry* 2014, 53, 8021−8030

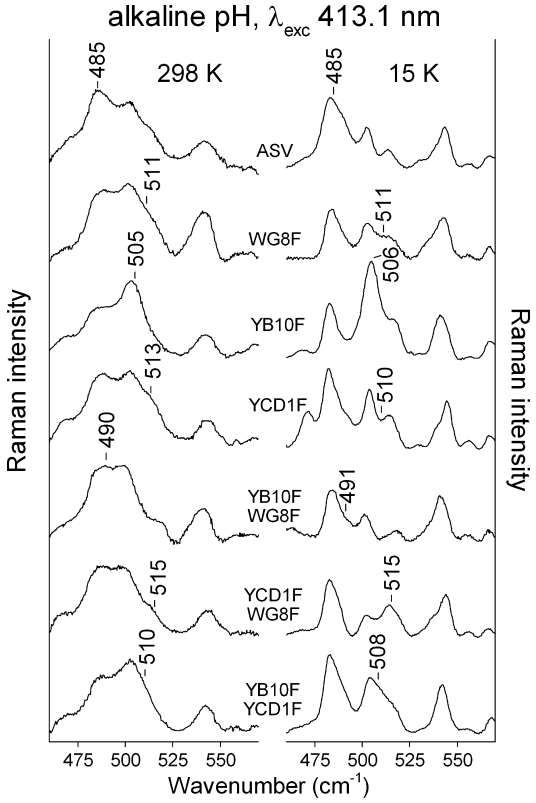

Figure 4. Comparison of the low-frequency region RR spectra of ASV and its mutants at pH 9.8, except for WG8F-YB10F and WG8F-YCD1F (pH 9.1) at 298 K (left) and 15 K (right). The frequency of the ν(Fe−OH) stretching mode, obtained from the curve-fitted spectra (see Materials and Methods and Figure S7, Supporting Information), is noted for each spectrum. Experimental conditions: 413.1 nm laser excitation, 1 cm^{-1} spectral resolution; ASV: (298 K) 10 mW laser power at the sample; average of 5 spectra with 600 s integration time; (15 K) 14 mW laser power at the sample; average of 2 spectra with 1200 s integration time. WG8F: (298 K) 14 mW laser power at the sample; average of 8 spectra with 600 s integration time; (15 K) 15 mW laser power at the sample; average of 5 spectra with 360 s integration time. YB10F: (298 K) 15 mW laser power at the sample; average of 8 spectra with 1000 s integration time; (15 K) 15 mW laser power at the sample; average of 2 spectra with 2700 s integration time. YCD1F: (298 K) 17 mW laser power at the sample; average of 4 spectra with 1200 s integration time; (15 K) 19 mW laser power at the sample; average of 4 spectra with 1800 s integration time. YB10F-WG8F: (298 K) 4 mW laser power at the sample; average of 9 spectra with 1500 s integration time; (15 K) 5 mW laser power at the sample; average of 18 spectra with 500 s integration time. YCD1F-WG8F: (298 K) 3 mW laser power at the sample; average of 6 spectra with 600 s integration time; (15 K) 12 mW laser power at the sample; average of 2 spectra with 3000 s integration time. YB10F-YCD1F: (298 K) 15 mW laser power at the sample; average of 2 spectra with 1800 s integration time; (15 K) 5 mW laser power at the sample; average of 2 spectra with 1800 s integration time.

oscillator. In fact, with an increase of the H-bond strength, a decrease of the force constant of the Fe−O bond together with a loss of its diatomic oscillator character (via vibrational coupling with the Fe−OH bending and torsion and the O−HX stretch modes) is expected. For example, it has been previously observed for alkaline horseradish peroxidase that the ν(Fe−OH) band moves to higher frequencies in D_2O than in H_2O.[8] Similar to HRPC, the band at 485 cm^{-1} in ASV upshifts by 4 cm^{-1} in D_2O (489 cm^{-1}) and downshifts to 471 cm^{-1} (−14 cm^{-1}) in $H_2{}^{18}O$, thus confirming the assignment to the ν(Fe−OH) stretching mode of the 6cLS form.[7] The corresponding band of the 6cHS has not been identified. The differences in the observed isotopic shifts with respect to the calculated values together with the remarkably low frequency, about 65 cm^{-1} lower than that observed for metMb and metHb,[8] indicates strong multiple hydrogen bonds between the OH^- and distal residues. In fact, with an increase of the H-bond strength, a decrease of the force constant of the Fe−OH^- bond with the concomitant decrease of the ν(Fe−OH) stretching frequency is expected. Accordingly, each mutation results in a different, but increased, ν(Fe−OH) stretching frequency (Table 2), with an isotopic shift that may be very different from the calculated values, probably as a consequence of the change in the H-bond strength.

Unlike the case of the fluoride ligand, where the frequency of the RR ν(Fe−F) stretching mode of YB10F variant was identical to that of the WT protein (5), in the present case, all of the singly mutated proteins show a similar, remarkable upshift (20−28 and 21−26 cm^{-1} at RT and LT, respectively) of the ν(Fe−OH) frequency resulting from the rupture of one H-bond interaction. Interestingly, the doubly mutated variant, YB10F-YCD1F, in which both distal Tyr residues are missing, also gives rise to a similar result. Conversely, the results obtained for the YB10F-WG8F and YCD1-WG8F doubly mutated variants are quite different. In particular, in the YB10F-WG8F mutant (i.e., in the presence of YCD1 as the only putative H-bond donor), the ν(Fe−OH) frequency is comparable to that of WT, indicating a rearrangement of the residue and a strong H-bond interaction. In contrast, in theYCD1-WG8F mutant (i.e., in the presence of only YB10 as potential H-bond donor), the highest frequency upshift among all the variants (30 cm^{-1}) is observed, thus indicating the weakest H-bond interaction to the hydroxo ligand among the three distal polar residues.

A structural analysis of the nearby environment of both tyrosine distal residues, depicted in Figure 5, shows that the surroundings of YB10 are polar and highly hydrated. Moreover, an Arg side chain persistently appears in close vicinity of YB10 during the time scale of the MD simulation (mean value of RE10-YB10 distance of about 4.7 Å). The same scenario was observed for all mutated forms of Tf-trHb that retain YB10. Conversely, the surroundings of YCD1 are hydrophobic and nonhydrated, where the closest residues VB13 and LC1 determine the boundary of the distal cavity, suggesting that pK_a values for both tyrosine residues must be different.

Accordingly, molecular dynamics simulations show that, if deprotonated, YCD1 swings out of the distal heme cavity to the protein surface and maintains such a position for the entire time scale of the simulation (Figure 6A). This finding suggests that YCD1 needs to be protonated to remain in the distal cavity. Furthermore, the MC4 residue moves into the structurally conserved CD1 position, which also strongly suggests that a deprotonated YCD1 is not a realistic scenario. Conversely, in the case of deprotonated YB10, the structure exhibits an OH^- ligand stabilized by the distal residues, and YB10 remains in the distal side during the time scale of our simulation (Figure 6B). These structural considerations and the experimental data allow us to conclude that, even at slightly alkaline pH values, YB10 may be deprotonated. Two independent simulations of 200 ns each have been performed to support this hypothesis, which gave similar results. Figure 7 shows the time evolution, during the time scale of one of the

dx.doi.org/10.1021/bi501132a | Biochemistry 2014, 53, 8021−8030

Table 2. RR Frequencies of the 6cLS ν(Fe−OH) Stretching Mode in H_2O, D_2O, and $H_2{}^{18}O$ Observed at 298 K (RT) and 15 K (LT) for ASV and Mutated Proteins[a]

	RT			LT		
	H_2O	D_2O	$H_2{}^{18}O$	H_2O	D_2O	$H_2{}^{18}O$
WT/ASV	485	489 (+4) [−10]	471(−14) [−20]	485	489 (+4) [−10]	471 (−14) [−20]
WG8F	511	498 (−13) [−11]	489 (−22) [−21]	511	499 (−12) [−11]	488 (−23) [−21]
YB10F	505	496 (−9) [−11]	486 (−19) [−21]	505	493 (−12) [−11]	487 (−18) [−21]
YCD1F	513	501 (−12) [−11]	489 (−24) [−21]	510	501 (−9) [−11]	487 (−23) [−21]
YB10F-WG8F	490	485 (−5) [−11]	485 (−5) [−20]	491	480 (−11) [−11]	483 (−8) [−20]
YCD1F-WG8F	515	501 (−14) [−11]	489 (−26) [−21]	515	500 (−15) [−11]	500 (−15) [−21]
YB10F-YCD1F	510	498 (−12) [−11]	485 (−25) [−21]	508	494 (−14) [−11]	486 (−22) [−21]

[a]Determined on the basis of their curve-fitted spectra (see Figure S7, Supporting Information). The observed isotopic shifts are reported in parentheses, and the expected isotopic shifts, in square brackets, calculated on the basis of the diatomic harmonic oscillator model.

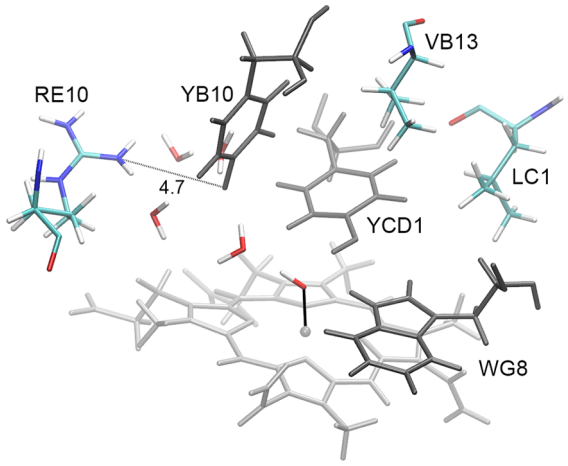

Figure 5. Schematic representation of the environment of both tyrosine distal residues. Polar and highly hydrated vs a hydrophobic and nonhydrated surroundings are observed for YB10 and YCD1, respectively. The distal triad WG8, YB10, and YCD1 is shown in gray. Note the Arg residue close to YB10 (RE10 at ∼4.7 Å).

simulations, of the HO−O_{YB10}(blue), OH−O_{WG8} (red), and OH−O_{YCD1} (green) distances of WT Tf-trHb following deprotonation of YB10. During the 200 ns of the simulation, the distal heme cavity undergoes swapping among several conformations involving one or two water molecules bridging the deprotonated YB10 to the hydroxyl-coordinated ligand.

The presence of two conformations, each exhibiting three H-bonds between distal residues and the hydroxo ligand that acts as an acceptor, had been proposed previously for WT Tf-trHb when both tyrosines (YB10 and YCD1) were considered to be protonated.[7] Although these conformations may exist, we believe that at alkaline pH they are less populated than those observed when YB10 is deprotonated. Accordingly, the MD simulations of the WT form containing a deprotonated YB10 residue show conformations where the OH^- ligand is acting as acceptor of direct H-bonds with TrpG8 and YCD1, whereas YB10 is H-bonded to one or two water molecules, one of which is H-bonded to the OH^- ligand as donor. This conformation is characterized by H-bonds that stabilize the OH^- ligand (Figure 8) more favorably than the case when both tyrosines are protonated (see Figure 5 in ref 7).

Upon mutation, MDS shows that in the singly mutated protein the hydroxo ligand is stabilized in a similar manner as that in the WT protein, although necessarily lacking an H-bond (Figure 9A−C). Interestingly, in the double mutants, in agreement with the RR Fe−OH^- stretching frequency, only one H-bond is maintained with OH^- in the presence of YB10 alone (YCD1F-WG8F mutant) through a H-bonded water molecule. In contrast, water molecules enter the cavity to stabilize the hydroxo ligand together with the WG8 (YB10F-YCD1F mutant) or YCD1 residue (YB10F-WG8F mutant). In the latter case, the H-bonds appear to be favored by the very short distances with the oxygen atom, consistent with the very low RR frequency of the ν(Fe−OH) stretching mode and similar to that observed for the WT protein.

Figure 10 compares the LS EPR signals of ASV and its distal mutants at alkaline pH. As noted previously for the WT protein and triple mutant (YB10F-YCD1F-WG8F),[7] the relative intensities of the HS signals of the mutants become considerably reduced at alkaline pH, whereas the LS signals

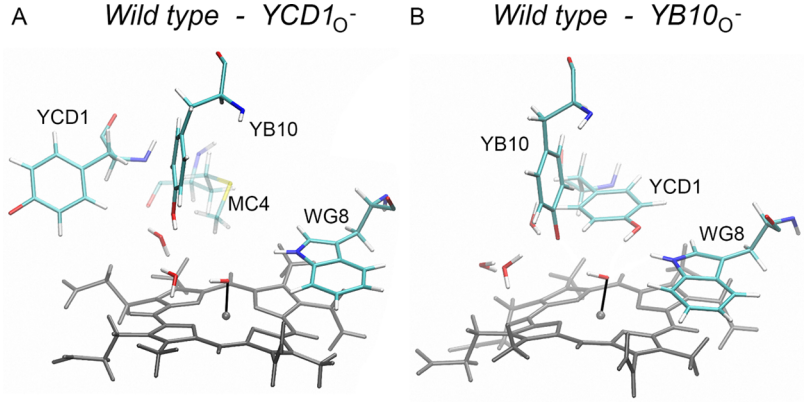

Figure 6. Schematic representation of the distal heme cavity of WT Tf-trHb following the deprotonation of YCD1 (A) and YB10 (B).

dx.doi.org/10.1021/bi501132a | Biochemistry 2014, 53, 8021−8030

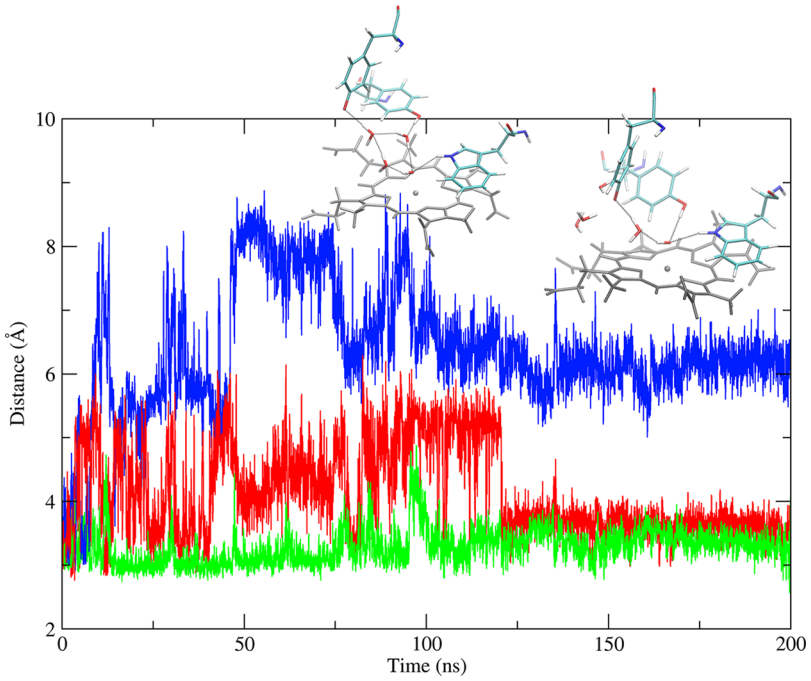

Figure 7. MD simulation showing structural rearrangements over 200 ns of the heme cavity of WT Tf-trHb at alkaline pH, following YB10 deprotonation, of the HO−O_{YB10}(blue), OH−N_{WG8} (green), and OH−O_{YCD1} (red) distances.

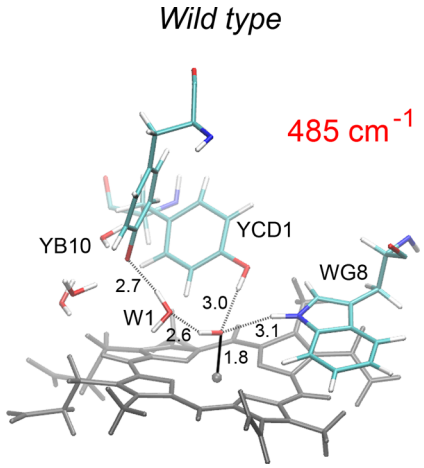

Figure 8. Schematic representation of the distal heme cavity of WT Tf-trHb at alkaline pH showing, on the basis of MD simulations, the H-bond network (dotted lines) stabilizing the iron-bound OH^-. Distances are in angstroms. YB10 is deprotonated. The corresponding ν(Fe−OH) stretching mode frequency is shown in red.

are enhanced by approximately 10-fold (data not shown). The two double mutants, YB10F-WG8F and YCD1F-WG8F, are the exception to this behavior. As noted also for the RR spectra at RT and 15 K (Figure 3; Figure S6, Supporting Information), an increase of a 5cHS species is observed for these mutants, giving rise to a more rhombic $g_\perp$ signal compared to that for ASV (Figure S5B, Supporting Information). The line width (ca. 100 G) is approximately double that observed for the spectra at pH 6; nevertheless, the line shape is quite different from the broad signal observed for free heme, suggesting that it does not result from heme dissociated from the protein. The line broadening, likely due to g strain[15,16] as well as the presence of several LS species deriving from different conformers, may be caused by local structural flexibility induced by the absence of both the WG8 and a Tyr residue. Furthermore, the appearance of the 5cHS state suggests that, in the absence of the Trp and a Tyr residue, a higher flexibility allows the OH^- ligand to move away from the heme iron atom.

On the basis of previously reported hydroxyl complexes (Table 3), the LS species with g_1 in the range 2.7−2.8 are assigned to His/OH^- coordination, where the OH^- group is strongly H-bonded. Moreover, at alkaline pH, the mutants involving WG8 substitution show signals with $g > 3$ that disappear at pH 6 (Figure 2). This observation suggests that these signals must result from His/OH^- coordination or from perturbation of distal cavity properties at alkaline pH values only. They are, however, difficult to explain on the basis of literature data, since such signals have been assigned to His/His or His/Lys coordination (Table 3), which are inconsistent with the amino acid side chain distribution of Tf-trHb that lacks both His or Lys inside or in the close proximity of the distal cavity. However, it cannot be ruled out that at alkaline pH the structural instability described above for these mutants allows an internal ligand to bind the heme iron, but it must be noted that the alkaline transitions are fully reversible and that no denaturation has been observed. The apparent absence in the RR spectrum of multiple LS forms observed in the EPR spectrum, particularly for mutants involving WG8 substitution, is likely due to the additional forms having very similar RR frequencies.

The g values and assignments of the various Tf-trHb LS signals are reported in Table 4. As noted above, the ν(Fe−OH) frequency of ASV is 65 cm^{-1} lower than that of metMb, indicating a reduced force constant of the Fe−OH^- bond. This is consistent with the determination of the tetragonality (Δ/λ) and rhombicity (V/Δ) parameters derived from the respective g values[15,17] for the two cases (Table 4). The tetragonality of alkaline ASV (5.40) is lower than that of the corresponding form of metMb (6.62) and, hence, indicates a lengthening of the Fe−OH^- bond with consequent reduction of the axial

dx.doi.org/10.1021/bi501132a | *Biochemistry* 2014, 53, 8021−8030

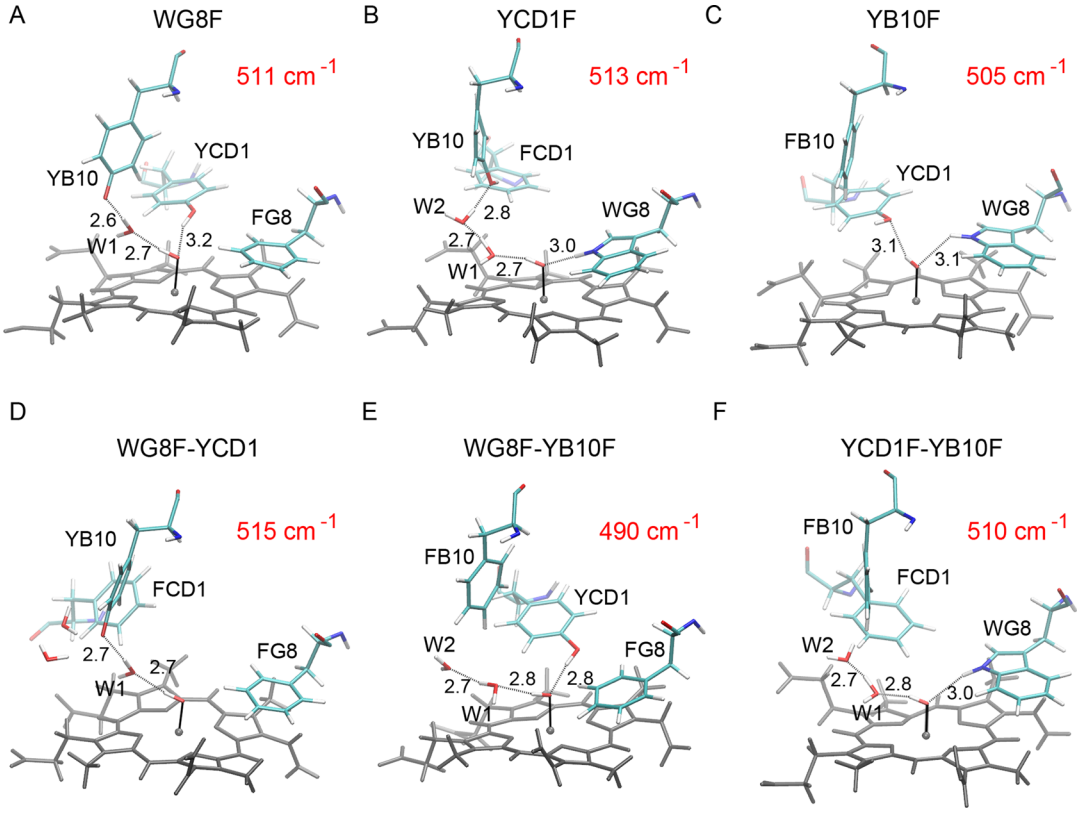

Figure 9. Schematic representation of the distal heme cavity of the mutated proteins at alkaline pH showing, on the basis of MD simulations, the hydrogen-bond network (dotted lines) stabilizing the iron-bound OH^- for single (A–C) and double (D–F) mutant proteins. TyrB10 being deprotonated, acts as a H-bond acceptor, whereas WG8 and YCD1 are H-bond donors. Distances are in angstroms. The corresponding ν(Fe–OH) stretching mode frequencies are shown in red.

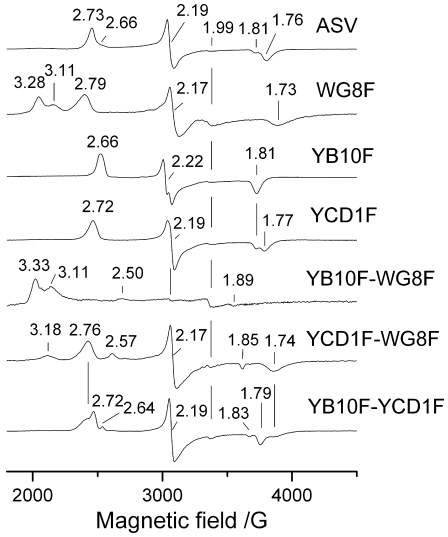

Figure 10. X-band EPR spectra of Tf-trHb and mutants at pH 9.8, except for WG8F-YB10F and WG8F-YCD1F (pH 9.1), in 0.1 M glycine. The spectra were recorded at 5 K, 1 mW microwave power, and 10 G modulation amplitude. Spectra have been shifted along the ordinate axis to allow better visualization. g values are indicated.

ligand field strength. In general, the tetragonality (Δ/λ) of the mutants determined from the g values for the intense EPR species is greater than that of ASV. This is consistent with the increase in the RR ν(Fe–OH) frequencies observed for the mutants and a shortening of the Fe–OH^- bond, with consequent increase of the axial ligand field strength (Tables 2 and 4).

CONCLUSIONS

The present results offer a detailed structural and spectroscopic picture of the heme iron-bound hydroxyl ligand in Tf-trHb. The distal triad WG8, YB10, and YCD1 in wild-type Tf-trHb can provide multiple H-bonding options with the iron bound ligand, in terms of both donor and acceptor modality. These options are, however, strongly dependent on the type of ligand. As clearly outlined in the present work, when the ligand is a hydroxyl group, endowed with both H-donor or acceptor properties, the interplay between the distal triad and the hydroxyl group is manifold.

The opportunities offered by the current set of combinatorial mutants have enabled the relative importance of the H-bonding interactions between the distal triad (WG8, YCD1, and YB10) in wild type and the iron-bound ligand to be assessed. The water ligand is a very weak H-bond donor and is easily deprotonated at slightly alkaline pH values. Thus, the N proton of TrpG8 residue represents the dominant H-bonding contribution to the exogenous ligand, in agreement with the downshift of the pK_a value of the hydroxyl moiety by 1 unit at least.

Interestingly, at variance with fluoride ligand investigated previously, both tyrosines have been shown to be involved in the stabilization of the hydroxo ligand, although the participation of YB10 may occur as a phenolate ion and through interposed water molecules. Nevertheless, as suggested by the MD simulations, the role of neighboring distal pocket

dx.doi.org/10.1021/bi501132a | Biochemistry 2014, 53, 8021–8030

Table 3. Comparison of the EPR Spectral Parameters of Various Low-Spin Heme Proteins

protein[a]	g_1	g_2	g_3	pH	coordination	ref
HRPA2	2.96	2.13	1.66	alkaline	His/OH^{-b}	18
HHMb	2.55	2.17	1.85	alkaline	His/OH^-	19
L. pectinata Hb II	2.61	2.20	1.82	alkaline	His/OH^-	19
S. marcescens HasA	2.85	2.21	1.71	7.5	His/Tyr^{-b}	20, 21
HSA ibuprofen	2.93	2.27	1.55	6.9	His/Tyr^{-b}	22
L. pectinata Hb II	2.76	2.20	1.75	alkaline	His/Tyr^-	19
various heme proteins[c]	~2.8	2.4	1.5		His/His	23, 24
cytochrome b	>3				His/His[d]	25
HH cytochrome c	3.06	2.25	1.25	7.0	Met/His	24
Euglena cytochrome	3.20	2.05	1.39	7.0	Met/His[e]	24
HH cytochrome c	3.37	2.1		alkaline	Lys/His	24
HH cytochrome c	3.58			alkaline	Lys/Lys	24

[a]$HRPA_2$, horseradish peroxidase isoenzyme A_2; HH, horse heart; HSA, human serum albumin. [b]OH^- strongly H-bonded. [c]Approximate g values. [d]Imidazole planes, nonparallel. [e]Imidazole with enhanced H-bonding.

Table 4. EPR Spectral Parameters of Tf-trHb and Mutants at Alkaline pH[a]

protein	ν(Fe−OH)	g_1	g_2	g_3	intensity[a]	coordination	Δ/λ	V/Δ
WT/ASV	485	2.73	2.19	1.76	s	His/OH^{-b}	5.40	0.48
		2.66	2.19	1.81	vw	His/OH^-		
WG8F	511	2.79	2.17	1.73	s	His/OH^{-b}	5.49	0.44
		3.28[c]			s	His/OH^{-b}		
		3.11[c]			w	His/OH^{-b}		
YB10F	506	2.66	2.22	1.81	s	His/OH^-	5.38	0.55
YCD1F	510	2.72	2.19	1.77	s	His/OH^{-b}	5.50	0.48
YB10F-WG8F	491	3.33[c]			s	His/OH^{-b}		
		3.11[c]			s	His/OH^{-b}		
		2.50	2.19	1.89	vw	His/OH^-		
YCD1F-WG8F	515	2.76	2.17	1.74	s	His/OH^{-b}	5.53	0.45
		2.57	2.17	1.85	w	His/OH^-		
		3.18[c]			w	His/OH^{-b}		
YB10F-YCD1F	508	2.76	2.17	1.74	s	His/OH^{-b}	5.53	0.45
		2.72	2.19	1.79	s	His/OH^{-b}	5.81	0.47
		2.64	2.19	1.83	w	His/OH^-		
HRPA2[d]	512	2.93	2.13	1.66		His/OH^{-b}	5.55	0.36
Mb[e]	550	2.55	2.17	1.85		His/OH^-	6.62	0.53

[a]s, strong; w, weak; vw, very weak. [b]OH^- strongly H-bonded. [c]Such high g values have not been reported previously for His/OH^- coordination, even when the OH^- is strongly H-bonded. [d]Ref 18. [e]Refs 8 and 19. [a]The ν(Fe−OH) Raman frequencies obtained at 15 K (LT) are also reported (see Table 2).

side chains, such as residue RE10, might not be negligible and will need to be assessed by site-specific mutants.

More general conclusions can be drawn on the significance of the present findings over the vast population of group II truncated hemoglobins thus identified in microorganisms. The occurrence of WG8 and YB10 in conserved positions within the distal side has suggested that H-bond interactions to the iron-bound ligand may either lock the heme distal residues into conformations that limit ligand access to the heme distal pocket or promote proton transfer to the ligand in view of catalytic roles related to O_2/NO chemistry. The present work highlights the possibility that YB10 might well be involved in a proton relay mechanism operative in the catalytic processing of oxygen or NO related species, thus adding another piece to the puzzle underlying the biochemical role of these proteins. Nevertheless, robust catalytic activity regarding NO or oxygen reactive species detoxification has been demonstrated only for a few group II truncated hemoglobins.[26] Furthermore, the heterogeneity of the distal sites, which vary in terms of their accessibility, local structures, polarity, and ligand stabilization mechanisms, leaves open questions regarding their genuine physiological roles.

■ ASSOCIATED CONTENT

Supporting Information

Time evolution of RMSD for backbone atoms in the mutant forms of Tf-trHb (S1 and S2), titration curves (S3), UV−vis electronic absorption spectra at pH 6.0 (S4), X-band EPR spectra (S5), high-frequency RR spectra obtained at 15 K (S6), curve-fit low-frequency RR spectra at room and low temperature (S7). This material is available free of charge via the Internet at http://pubs.acs.org.

■ AUTHOR INFORMATION

Corresponding Author

*E-mail: giulietta.smulevich@unifi.it; Phone: (+39) 0554573083.

Present Address

[▽](F.P.N.) Sanofi, Viale Bodio 37, I-20158 Milano, Italy.

Author Contributions

[○]F.P.N. and J.P.B. contributed equally to this work.

Funding

This work was supported by the Institute Pasteur Fondazione Cenci Bolognetti (A. Boffi), MIUR FIRB RBFR08F41U_002 (A. Bonamore), MIUR PRIN 2008BFJ34 (A. Feis and A. Boffi), University of Buenos Aires, ANPCYT PICT 06-1266, and European Union FP7 project NO Stress (D. Estrin), and the Italian Ministero dell'Istruzione, dell'Università e della Ricerca (MIUR), Direzione Generale per l'Internazionalizzazione della Ricerca, Progetti di Grande Rilevanza Italia-Argentina.

Notes

The authors declare no competing financial interest.

■ ABBREVIATIONS

trHb, truncated hemoglobin; Tf, *Thermobifida fusca*; HRPC, horseradish peroxidase isoenzyme C; Mb, myoglobin; WT, wild type; ASV, acidic surface variant of Tf-trHb containing single-site mutations Phe107Glu and Arg91Glu; MES, 2-(*N*-morpholino)ethanesulfonic acid; MD, molecular dynamics; EPR, electron paramagnetic resonance; RR, resonance Raman; 5c, five-coordinate; 6c, six-coordinate; HS, high spin; LS, low spin; RMSD, root-mean-square displacements; RESP, restricted electrostatic potential recipe; DFT, density functional theory; PBE, Perdew–Burke–Ernzerhof

■ REFERENCES

(1) Capece, L., Boechi, L., Perissinotti, L. L., Arroyo-Mañez, P., Bikiel, D. E., Smulevich, G., Marti, M. A., and Estrin, D. A. (2013) Small ligand–globin interactions: reviewing lessons derived from computer simulation. *Biochim. Biophys. Acta 1834*, 1722–1738.

(2) Bonamore, A., Ilari, A., Giangiacomo, L., Bellelli, A., Morea, V., and Boffi, A. (2005) A novel thermostable hemoglobin from the actinobacterium *Thermobifida fusca*. *FEBS J. 272*, 4189–4201.

(3) Droghetti, E., Nicoletti, F. P., Bonamore, A., Boechi, L., Arroyo-Mañez, P., Estrin, D. A., Boffi, A., Smulevich, G., and Feis, A. (2010) Hemepocket structural properties of a bacterial truncated hemoglobin from *Thermobifida fusca*. *Biochemistry 49*, 10394–10402.

(4) Droghetti, E., Nicoletti, F. P., Bonamore, A., Sciamanna, N., Boffi, A., Feis, A., and Smulevich, G. (2011) The optical spectra of fluoride complexes can effectively probe H-bonding interactions in the distal cavity of heme proteins. *J. Inorg. Biochem. 105*, 1338–1343.

(5) Nicoletti, F. P., Droghetti, E., Boechi, L., Bonamore, A., Sciamanna, N., Estrin, D. A., Feis, A., Boffi, A., and Smulevich, G. (2011) Fluoride as a probe for H-bonding interactions in the active site of heme proteins: the case of *Thermobifida fusca* hemoglobin. *J. Am. Chem. Soc. 133*, 20970–20980.

(6) Nicoletti, F. P., Comandini, A., Bonamore, A., Boechi, L., Boubeta, F. M., Feis, A., Smulevich, G., and Boffi, A. (2010) Sulfide binding properties of truncated hemoglobins. *Biochemistry 49*, 2269–2278.

(7) Nicoletti, F. P., Droghetti, E., Howes, B. D., Bustamante, J. P., Bonamore, A., Sciamanna, N., Estrin, D. A., Feis, A., Boffi, A., and Smulevich, G. (2013) H-bonding networks of the distal residues and water molecules in the active site of *Thermobifida fusca* hemoglobin. *Biochim. Biophys. Acta 1834*, 1901–1909.

(8) Feis, A., Marzocchi, M. P., and Smulevich, G. (1994) Spin state and axial ligand bonding in the hydroxide complexes of metmyoglobin, methemoglobin, and horseradish peroxidase at room and low temperatures. *Biochemistry 33*, 4577–4583.

(9) Asher, S. A., Vickery, L. E., Schuster, T. M., and Sauer, K. (1977) Resonance Raman spectra of methemoglobin derivatives. selective enhancement of axial ligand vibrations and lack of an effect of inositol hexaphosphate. *Biochemistry 16*, 5849–5856.

(10) Asher, S. A., and Schuster, T. M. (1979) Resonance Raman examination of axial ligand bonding and spin-state equilibria in metmyoglobin hydroxide and other heme derivatives. *Biochemistry 18*, 5377–5387.

(11) Egawa, T., and Yeh, S.-R. J. (2005) Structural and functional properties of hemoglobins. *Inorg. Biochem. 99*, 72–96.

(12) Ikeda-Saito, M., Hori, H., Andersson, L. A., Prince, R. C., Pickering, I. J., George, G. N., Sanders, C. R., Lutz, R. S., McKelvey, E. J., and Mattera, R. (1992) Coordination structure of the ferric heme iron in engineered distal histidine myoglobin mutants. *J. Biol. Chem. 267*, 22843–22852.

(13) Lukat-Rodgers, G. S., and Rodgers, K. R. (1998) Spin-state equilibria and axial ligand bonding in FixL hydroxide: a resonance Raman study. *J. Biol. Inorg. Chem. 3*, 274–281.

(14) Brunori, M., Amiconi, G., Antonin, E., Wyman, J., Zito, R., and Fanelli, A. R. (1968) The transition between 'acid' and 'alkaline' ferric heme proteins. *Biochim. Biophys. Acta 154*, 315–322.

(15) Palmer, G. (1985) The electron paramagnetic resonance of metalloproteins. *Biochem. Soc. Trans. 13*, 548–560.

(16) Hagen, W. R. (1981) Dislocation strain broadening as a source of anisotropic linewidth and asymmetrical lineshape in the electron paramagnetic resonance spectrum of metalloproteins and related systems. *J. Magn. Reson. 44*, 447–469.

(17) Taylor, C. P. S. (1977) The EPR of low spin heme complexes. Relation of the t2g hole model to the directional properties of the g tensor, and a new method for calculating the ligand field parameters. *Biochim. Biophys. Acta 491*, 137–149.

(18) Howes, B. D., Feis, A., Indiani, C., Marzocchi, M. P., and Smulevich, G. (2000) Formation of two types of low-spin heme in horseradish peroxidase isoenzyme A2 at low temperature. *J. Biol. Inorg. Chem. 5*, 227–235.

(19) Kraus, D. W., Wittenberg, J. B., Lu, J. F., and Peisach, J. (1990) Hemoglobins of the *Lucina pectinata*/bacteria symbiosis. II. An electron paramagnetic resonance and optical spectral study of the ferric proteins. *J. Biol. Chem. 265*, 16054–16059.

(20) Izadi, N., Henry, Y., Haladjian, J., Goldberg, M. E., Wandersman, C., Delepierre, M., and Lecroisey, A. (1997) Purification and characterization of an extracellular heme-binding protein, HasA, involved in heme iron acquisition. *Biochemistry 36*, 7050–7057.

(21) Arnoux, P., Haser, R., Izadi, N., Lecroisey, A., Delepierre, M., Wandersman, C., and Czjzek, M. (1999) The crystal structure of HasA, a hemophore secreted by *Serratia marcescens*. *Nat. Struct. Biol. 6*, 516–520.

(22) Nicoletti, F. P., Howes, B. D., Fittipaldi, M., Fanali, G., Fasano, M., Ascenzi, P., and Smulevich, G. (2008) Ibuprofen induces an allosteric conformational transition in the heme complex of human serum albumin with significant effects on heme ligation. *J. Am. Chem. Soc. 130*, 11677–11688.

(23) Blumberg, W. E., and Peisach, J. (1971) Probes of enzymes and hemoproteins, in *Probes of Structure and Function of Macromolecules and Membranes* (Yonetani, T., Mildvan, A. S., and Chance, B., Eds.) pp 215–228, Academic Press, New York.

(24) Brautigan, D. L., Feinberg, B. A., Hoffman, B. M., Margoliash, E., Peisach, J., and Blumberg, W. E. (1977) Multiple low spin forms of the cytochrome c ferrihemochrome. EPR spectra of various eukaryotic and prokaryotic cytochromes c. *J. Biol. Chem. 252*, 574–582.

(25) Walker, F. A., Huynh, B. H., Scheidt, W. R., and Osvath, S. R. (1986) Models of the cytochromes b. Effect of axial ligand plane orientation on the EPR and Moessbauer spectra of low-spin ferrihemes. *J. Am. Chem. Soc. 108*, 5288–5297.

(26) Ascenzi, P., di Masi, A., Tundo, G. R., Pesce, A., Visca, P., and Coletta, M. (2014) Nitrosylation mechanisms of *Mycobacterium tuberculosis* and *Campylobacter jejuni* truncated hemoglobins N, O, and P. *PLoS One 9*, e102811.